JOURNAL OF GEOPHYSICAL RESEARCH, VOL. 87, NO. B2, PAGES 990-1000, FEBRUARY 10, 1982

SHEAR FRACTURE ENERGY OF WESTERLY GRANITE FROM POST-FAILURE BEHAVIOR

Teng-fong Wong

Department of Earth and Planetary Sciences, Massachusetts Institute of Technology, Cambridge, Massachusetts 02139

Abstract. We consider in this paper the energetic relationship among four different types of measurements: evaluation of shear fracture energy from seismological data, rock mechanics study of post-failure behavior in triaxial compression, measurement of specific surface energy of minerals in a tensile mode, and scanning electron microscope (SEM) observation of stress-induced microstructures. Shear fracture energy can be estimated from post-failure deformation data following an integration scheme recently suggested by Rice. Values so determined for Westerly granite at pressures up to 250 MPa and temperatures up to 700°C are of the order of 10^4 J m^{-2}, which is about 2 orders of magnitude higher than the tensile values. Analysis of our data, together with previous room temperature post-failure data, show that the influence of temperature, pressure, and rock type can change the shear fracture energy by an order of magnitude. Microcracking energy can be estimated by multiplying the stress-induced crack area (obtained by stereological technique) and the single-crystal specific surface energy. Energy for the extension of microcracks resolvable under SEM can account for a major portion of the total energy input for pre-failure deformation. However, for post-failure deformation the estimate of microcracking energy is smaller than the total by at least an order of magnitude.

Introduction

One of the important goals of both seismology and rock mechanics is a better understanding of faulting. Seismologists have traditionally characterized the faulting process by a number of 'source parameters,' such as permanent slip, rupture velocity, or rise time, the values of which are determined through inversion of seismic data. Such an approach has greatly enhanced our understanding of certain aspects of the seismic source, but it has a major shortcoming of being only a kinematic description: the parameters are not directly related to the physics of the rupture process, and some of the slip functions, although they can fit observations, are physically unacceptable [Aki and Richards, 1980].

To address the source dynamics directly, one is hampered by the limited knowledge of the actual failure process. Nevertheless, a number of theoretical results have been obtained by adapting techniques from fracture mechanics and assuming physically plausible fracture criteria. These have helped to establish a more precise conceptual framework for the analyses of the source mechanism. As reviewed by Freund [1979], Aki and Richards [1980], and Rudnicki [1980], such an approach has been shown to be useful on a number of dynamic and quasi-static problems in fault mechanics.

A fundamental quantity used in all these models is the shear fracture energy or critical energy release rate under mode II loading. The quantity is commonly referred to as G_{IIc} in fracture mechanics literature; for convenience of notation we will simply refer to the parameter as G in this paper when no ambiguity arises. Physically, this quantity represents the energy flux for 'breakdown' processes at a crack tip and is the crucial parameter that constrains the energetics at the crack tip [Rice, 1980]. Lacking detailed knowledge of the rupture process, the value of G is the minimum amount of information required for any meaningful modeling of the source dynamics.

Unfortunately, laboratory studies to date have not been of much help in placing bounds on the magnitude of the shear fracture energy. With engineering applications in mind, most fracture mechanics techniques have been developed for the tensile mode or mode I [Freiman, 1979]. Likewise, the measurements on minerals and rocks are done in tension (Table 1b). Rice [1980] recently suggested that the shear G can be evaluated by performing an appropriate integration under the post-failure stress-displacement curve. He further showed that values so determined from room temperature data are closer to seismologically inferred values (Table 1a) than the laboratory measurements obtained in tension, although a maximum discrepancy of 3 orders of magnitude may still exist.

Can temperature effect account for this discrepancy? Or perhaps the effects of pressure and strain rate? It would clearly be of interest to apply the technique to a variety of rocks under geologically significant conditions. We have recently completed a series of experiments on the post-failure behavior of Westerly granite at temperature to 700°C and pressure to 250 MPa [Wong, 1981a]; here we shall discuss the results on G as determined from our data using Rice's scheme and compare the values with others evaluated from existing room temperature post-failure data.

If G so determined truly represents the shear fracture energy for the failure processes, a portion of it should be attributed to processes associated with microcracking. The G values determined by Rice for both intact and pre-fractured samples at room temperature were of the order of 10^4 J m^{-2} (Table 2), whereas previous measurements invariably showed that the tensile fracture energy for minerals is of the order of 1-10 J m^{-2} and for pre-cracked rock samples of the order of 10-100 J m^{-2} (Table 1b). An estimate of the microcrack surface area created in the post-failure stage for triaxial compression tests is available from our previous scanning

Paper number 1B1502.
0148-0227/82/001B-1502$01.00

TABLE 1a. Fracture Energy G: Seismological Estimate

G J m^{-2}	Method	Reference
10^7	from rupture propagation time	Takeuchi and Kikuchi [1973]
10^7	from strong motion data (maximum velocity and acceleration)	Ida [1973]
10^2	from spatial distribution of slip during fault creep estimated from field data	Rice and Simons [1976]
10^1-10^4 'frictional' 10^4-10^4 'fresh fracture'	from stress drop and fault dimension	Husseini et al. [1976]
10^6-10^8	from rupture velocity; based on barrier model	Das [1976]
10^6-10^8	from stress drop and fault dimension estimated from strong motion data, spatial distribution of aftershocks, and geologic evidence	Aki [1979]
10^6	from geodetic data and earthquake recurrence rate for San Andreas	Rudnicki [1980]
10^3	from McGarr et al.'s [1979] seismic data for a South African gold mine	this study
10^6	from McGarr et al.'s [1979] determination of seismic moment and underground measurement of average slip	this study

electron microscope (SEM) work [Wong, 1981b]. This area multiplied by the single-crystal fracture energy gives an estimate of the total energy input for microcracking processes. How do the two energy terms compare? Can we gain some insight into the energetics of faulting in initially intact samples by making such a comparison?

In this paper we shall try to address these questions and hopefully further our understanding of the relationship between the tensile and shear fracture energy, and between laboratory measurements and seismologically inferred values.

Theory

Inelastic Energy Dissipation in Pre-Failure Region

To put the latter discussion of fracture energy in perspective, we first estimate the energy associated with pre-failure inelastic processes. Let the stress field be given by σ_{ij}. For an increment of strain $d\varepsilon_{ij}$, part of which (de_{ij}) is attributed to elastic deformation and the rest to inelastic deformation, energy input per unit volume for inelastic processes will be given by

$$dW = \sigma_{ij} \, (d\varepsilon_{ij} - de_{ij})$$

In a triaxial test, with maximum compression given by σ_1 and $\sigma_2 = \sigma_3 = P$ the above relation becomes

$$dW = \sigma_1 \, (d\varepsilon_1 - de_1) + 2P(d\varepsilon_3 - de_3)$$

$$= \sigma \, (d\varepsilon_1 - de_1) + P(d\varepsilon_v - de_v)$$

where the differential stress $\sigma = \sigma_1 - \sigma_3$, and the volumetric strain $\varepsilon_v = \varepsilon_1 + 2\varepsilon_3$, $e_v = e_1 + 2e_3$. Note that ε_v is positive for compression and negative for dilatation; compressive stress is taken to be positive.

For most brittle rocks, the onset of dilatancy marks the point beyond which $d\varepsilon_{ij}$ and de_{ij} are significantly different. Following the notation of Brace et al. [1966], if C' denotes the differential stress at the onset of dilatancy, C the

TABLE 1b. Fracture Energy: Laboratory Tensile Measurement

G, J m^{-2}	Method	Reference
1-10	single crystals under tension	Brace and Walsh [1962]
10-10^2	pre-cracked rock samples under tension	Atkinson [1979]

TABLE 2. Laboratory Measurement of Shear Fracture Energy $\underline{G}$

Sample	σ_3, MPa	T, °C	Fracture Angle	10^4 $\underline{G}$, J m^{-2}	$\tau^p - \tau^f$, GPa	$\overline{\Delta u}$, mm	ω_o,* m	Reference
				Fichtelgebirge Granite				
	470	room	36°†	4.5#	0.13	0.34	0.18	Rummel et al. [1978]
	55	room	36°†	4.7	0.11	0.44	0.29	Rummel et al. [1978]
	300	room	36°†	7.3	0.15	0.49	0.24	Rummel et al. [1978]
				Witwatersrand Quartzite				
	14	room	25°†	0.8	0.05	0.15	0.21	Spottiswoode [1980]
	28	room	25°†	1.3	0.08	0.16	0.14	Spottiswoode [1980]
				Oshima Granite				
452	room	room	25°†	1.0	0.06	0.17	0.20	Sano [1978]
				Westerly Granite				
	room	room	25°†	0.7	0.08	0.09	0.08	Wawersik and Brace [1971]
	room	room	25°†	0.8	0.08	0.10	0.09	Wawersik and Brace [1971]
	20	room	25°†	0.6	0.10	0.06	0.04	Wawersik and Brace [1971]
	20	room	25°†	0.8	0.11	0.07	0.05	Wawersik and Brace [1971]
	80	room	25°†	0.3	0.08	0.04	0.04	Wawersik and Brace [1971]
	80	room	25°†	0.7	0.10	0.07	0.05	Wawersik and Brace [1971]
PFW22	80	150	25°	3.3	0.14	0.24	0.12	this study
PFW23	80	350	31°	2.3	0.10	0.23	0.16	this study
PFW13	250	150	30°	5.1	0.15	0.34	0.16	this study
PFW16	250	350	31°	2.2	0.10	0.22	0.15	this study
PFW17§	250	350	30°	1.7	0.08	0.22	0.19	this study
PFW27§	250	350	32°	1.3	0.07	0.19	0.19	this study
MTW 7	250	550	34°	2.3	0.09	0.26	0.21	this study
MTW 8	250	668	38°	2.3	0.05	0.45	0.64	this study

* Calculated with the following input values: $\nu = 0.25$ and $\mu = 30$ GPa.
† Fracture angles assumed.
# Polished sawcut sample.
§ Calculated from post-creep failure curve.

fracture stress, and D the inelastic dilatation at failure, then the total inelastic energy input per unit volume in the pre-failure stage is given by

$$W = \int_{C'}^{C} \sigma (d\varepsilon_1 - de_1) - P \cdot D \qquad (1)$$

Determination of G From Post-failure Curve

Most previous studies of post-failure behavior interpreted the results in terms of a classification first proposed by Wawersik [Wawersik and Fairhurst, 1970; Wawersik and Brace, 1971], who showed that the post-failure response of certain rock types is so unstable that the load-displacement curves can actually turn over so far as to take on a positive slope. Wawersik categorized this type of behavior as class II, in contrast to the more stable class I behavior with persistently negative post-failure slope. Whereas class I behavior can be observed in a stable manner by using a sufficiently stiff machine, class II rocks will fail explosively even if the stiffness is infinitely high, unless steps are taken to servo-control the testing machine, either mechanically by a feedback loop [Hudson et al., 1971] or manually [Wawersik and Brace, 1971].

Such a classification of the post-failure behavior is in essence a scheme to differentiate between two types of machine-sample interaction in terms of the relative magnitudes of stiffness. Does a critical change in sample stiffness represent a qualitative transition in physical characteristics? It is generally accepted that the stiffness is the natural parameter for characterizing the elastic deformation in the testing system; for the rock sample, however, the situation is not so clear. The stiffness is a quantity that depends on the Young's modulus and sample geometry, and even for the pre-failure deformation it is generally accepted that the stress-inelastic volumetric strain curve is preferred to the axial stress-strain curve for characterizing the physical processes. For the post-failure deformation the strain field can be highly heterogeneous. Consider a sample stressed triaxially as shown in Figure 1. Previous microscope [Wawersik and Brace, 1971; Hallbauer et al., 1973; Wong, 1981b], acoustic emission [Lockner and Byerlee, 1978], and holography [Soga et al., 1978] studies have shown that close to the peak stress a localized zone F is formed at an angle θ to the maximum compression direction (σ_1).

The complexities involved in trying to pinpoint the onset of shear localization was discussed by Wong [1981c] in relation to the diffi-

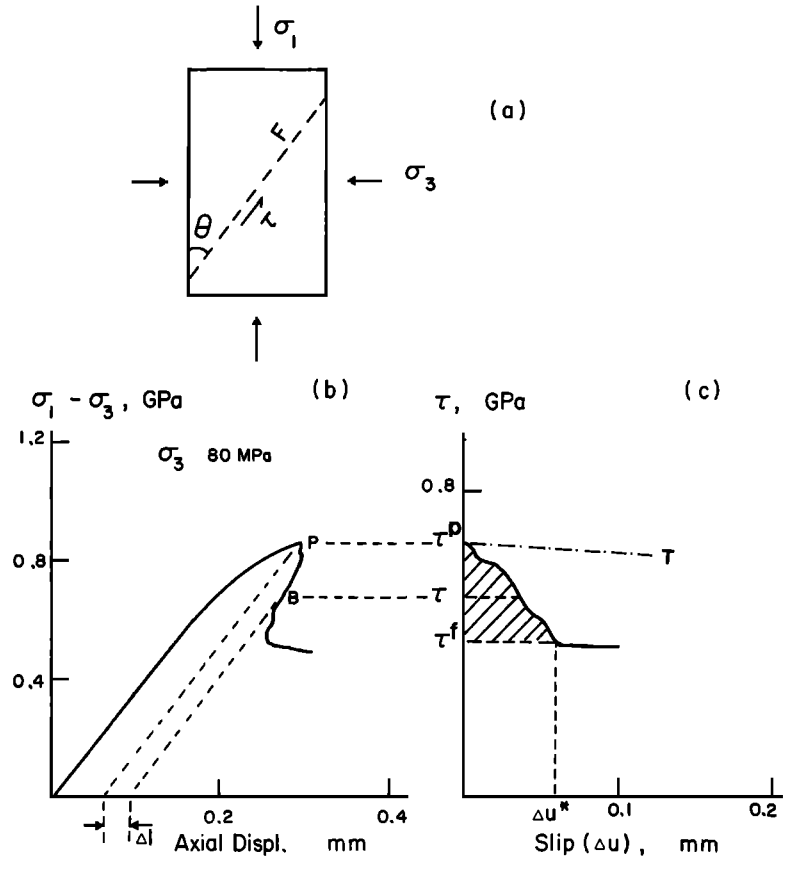

Fig. 1. (a) Shear localization of an initially intact sample stressed triaxially. (b, c) Transformation of post-failure data (of Westerly granite at 80 MPa and room temperature) to infer shear stress versus relative slip relation used in 'slip-weakening' model. The dash-dotted line marked T in Figure 1c shows the transition slope from class I to class II behavior.

culties in formulating a physically sound continuum model for brittle rock behavior. With this reservation in mind we shall assume for convenience in the analysis below that it occurs right at the peak stress.

Most of the deformation is taken up by shear along F, and it seems logical to characterize the post-failure processes by the stress and slip along the localized zone (which is, of course, the routine procedure for the analysis of friction in pre-fractured specimens). The shear traction along F (Figure 1a) is given by

$$\tau = \frac{\sigma_1 - \sigma_3}{2} \sin 2\theta$$

whereas the relative slip Δu at a point B (Figure 1b) can be expressed in terms of the post-failure axial displacement $\Delta \ell$ by

$$\Delta u = \Delta \ell / \cos \theta$$

The calculation of $\Delta \ell$ is based on the observation that up to the failure stress, the unloading response can be approximated by the elastic modulus in most cases [Wawersik and Brace, 1971]. At the high pressures we used, the initial loading curve is linear and can be used to estimate the modulus.

The transformation of a post-failure stress-strain record to a τ-Δu plot is outlined in Figures 1b and 1c. It can easily be shown that the transition from class I to class II occurs when the slope reaches the critical magnitude

$$(\tau/\Delta u) = (E/\ell) \sin^2\theta \cos \theta$$

where E is Young's modulus and ℓ the sample length. Within such a framework the slope of the τ-Δu curve is always negative, and the class I to class II transition is merely a gradual change.

The 'slip-weakening' concept has been proposed to model the mechanics of this broad class of materials for which the shear strength degrades with relative slip. Generalizing Barenblatt's [1962] 'cohesive zone' model originally intended for tensile cracks, Ida [1972] and Palmer and Rice [1973] independently suggested the use of analogous fracture mechanics ideas in the analysis of slip propagation under shear. Rice [1980] recently gave a succinct review of the topic; we will summarize the relevant results here.

The slip-weakening model (Figure 2) considers an earthquake fault as a shear crack with a peak shear strength τ^p. Relative slip initiates when the shear stress τ reaches τ^p, and the strength degrades from τ^p to a constant residual frictional strength τ^f as the slip Δu increases to a critical value Δu^*. Consequently, there is a 'breakdown zone' at the shear crack tip of dimen-

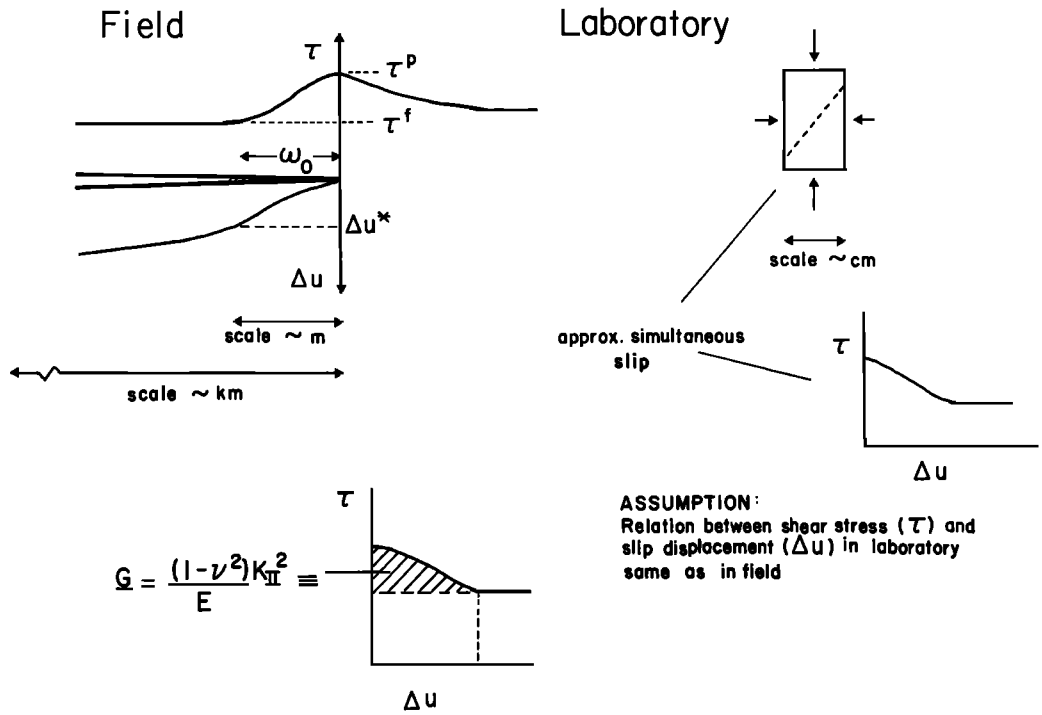

Fig. 2. Slip-weakening model as applied in the field and in the laboratory. The distribution of shear stress τ and slip displacement Δu with respect to a fault in the field is shown. The breakdown zone size ω_0 is also indicated.

sion ω_0 and with distribution of τ and Δu as shown on the left-hand side of Figure 2.

Applying the J integral [Rice, 1968] and assuming that ω_0 is small relative to the overall crack size, we can derive a criterion analogous to the critical energy release rate criterion in elastic fracture mechanics. The shear fracture energy or critical energy release rate (in mode II) is then given by

$$\underline{G} = \int_0^{\Delta u^*} [\tau(\Delta u) - \tau^f] \, d(\Delta u) \qquad (2)$$

A graphic representation of this relation is shown in Figure 2: $\underline{G}$ is simply the hatched area under the τ-Δu curve.

Rice [1980] pointed out that if the same τ versus Δu relation obtained in laboratory tests (Figure 1) applies in the field, then $\underline{G}$ can be estimated by performing a similar integral for the experimental data (Figure 2). Furthermore, estimates for breakdown zone size ω_0 and characteristic length of breakdown slip $\overline{\Delta u}$ are furnished by

$$\omega_0 = \frac{9\pi}{16(1-\nu)} \overline{\Delta u} \, \frac{\mu}{\tau^p - \tau^f} \qquad (3)$$

and

$$\underline{G} = (\tau^p - \tau^f) \, \overline{\Delta u} \qquad (4)$$

where μ and ν are shear modulus and Poisson's ratio, respectively.

Note that $\underline{G}$ in (2) differs from the shear fracture energy defined by Husseini et al. [1975] and Aki and Richards [1980] by a factor of 2. It is also different from the crushing energy G of McGarr et al. [1979], which was defined to be the total energy input by extending (1) to the post-failure region. They did not therefore take into consideration the localized nature of post-failure deformation. Also, $\underline{G}$ as defined in (2) does not include any contribution from the residual shear stress, since τ^f is explicitly subtracted from the integrand, whereas the crushing energy G does include this contribution.

Estimation of the Energy for Stress-Induced Cracking

If we have a means of estimating the surface area per unit volume (S_V) of stress-induced microcracks, the product of S_V with twice the specific surface energy for microcrack extension (2Γ) gives an estimate of energy input per unit volume for microcrack formation.

A direct measurement of S_V is not practical, since it would require three-dimensional observation of microcracks at high resolution. Most microscopic studies are performed on plane sections, and one has to resort to geometric probability theory [Kendall and Moran, 1963; Underwood, 1970] to estimate S_V from measurement of crack length per unit area (L_A) on sections. The measurement of L_A on SEM mosaics has been described elsewhere [Wong, 1981b], and the stereological formulae relating the SEM data to S_V were summarized by Wong [1981c].

For brittle deformation, most of the stress-induced cracks observed under SEM form in tension [Tapponnier and Brace, 1976; Kranz, 1979, 1980; Wong, 1981b] and therefore specific surface energy measurements on single crystals in the tensile mode [Brace and Walsh, 1962; Atkinson, 1979] are the appropriate values to input for Γ. However, at higher pressures and temperatures a larger portion of cracks at high angle

to σ_1 was observed, and many of these high-angle cracks show shear displacement in the post-failure stage [Wong, 1981b]. To our knowledge, no measurement of Γ in shear has been made. It was suggested by Friedman et al. [1972] that Γ for grain boundary cracks might be lower, but again no measurement is available. Nevertheless, it is unlikely that in either of these cases the value would be different from the tensile value by orders of magnitude.

If we denote the crack surface per unit volume in a virgin sample by S_V^0 and that in a pre-failure stressed sample by S_V, then the energy per unit volume for microcracking will be

$$M = 2\Gamma (S_V - S_V^0) \quad (5)$$

Let the crack surface per unit volume in a sample retrieved immediately after failure be S_V^f and that in a post-failure sample be S_V^p, the measurements being made in representative sections perpendicular to the localized zone. If the zone can be approximated by a planar zone with thickness w, then an estimate of the microcracking energy per unit area along the localized sone will be

$$M^1 = 2\Gamma (S_V^p - S_V^f)\, w \quad (6)$$

Note that M is in joules per cubic meter, whereas M^1 is in joules per square meter.

Determination of G of Earthquakes

Aki and Richards [1980], Rudnicki [1980], and Rice [1980] have discussed at some length how to determine $\underline{G}$ from seismological data. One formula frequently used is of the form

$$\underline{G} = \frac{R\,(\Delta\tau)^2}{\alpha\ \pi\ \mu} \quad (7)$$

where R is the characteristic radius of the fault, $\Delta\tau$ is the stress drop, and μ is the shear modulus. This is the equation used by both Husseini et al. [1975, 1976] and Aki [1979] to determine $\underline{G}$ for the Parkfield earthquake. α is a constant dependent on the details of the faulting process. Husseini et al. took $\alpha = 1$, whereas Aki determined α from a relationship involving the rupture velocity and the seismic compressional and shear velocities.

A number of techniques have been proposed for determining the input parameters in (7). Husseini et al. estimated the two parameters R and $\Delta\tau$ from seismic moment and corner frequency on the basis of Brune's [1970] model. Aki determined R from spatial distribution of aftershocks and assumption of existence of barriers along the fault and $\Delta\tau$ from strong motion data.

Approaches different from (7) can also be used; for example, Rice and Simons [1976] determined $\underline{G}$ from the spatial distribution of slip for a fault creep event, and Rudnicki [1980] determined $\underline{G}$ for the initiation of the 1857 California earthquake from geodetic data and historical record of earthquake recurrence time.

Results

Pre-failure Data

As shown in (1), to determine the inelastic energy input for pre-failure deformation, one needs measurements of both the axial and the volumetric strain; the latter was not monitored in our high-temperature experiments, and hence we can only consider room temperature results. Since some detailed SEM data are available from Tapponnier and Brace's [1976] study of Westerly granite at 50 MPa pressure, we will make the comparison on the basis of their data.

Following the notation of (1) and referring to Figure 1 of Tapponnier and Brace [1976], we have $C' = 250$ MPa, $C = 530$ MPa, $P = 50$ MPa, and $D = 3 \times 10^{-3}$. They did not show the axial stress-strain curve, but since the inelastic axial strain does not vary as much as D from sample to sample, we estimated the integral in (1) based on a similar experiment at $P = 51$ MPa and with $C' = 360$ MPa and $C = 620$ MPa. The integral was estimated to be 2.1×10^5 J m^{-3}, and substituting into (1) we obtain a value for W of 6×10^4 J m^{-3}. Brace et al. [1966] pointed out that the determination of C is accurate to a few percent, of C', 10–15%, and of D probably only to a factor of 2. Considering the additional error in computing the integral, we assign an uncertainty of 50% to the calculation of W.

We reproduce Tapponnier and Brace's SEM data on a virgin sample (T0) and a sample close to failure (T5) in Table 3. They counted the number of crack intersections per unit length with a set of parallel lines perpendicular ($P_L^{\perp}$) and parallel ($P_L^{\parallel}$) to σ_1. We have shown [Wong, 1981c] that the crack orientations in pre-failure samples can be approximated quite well with an axisymmetric distribution with one

TABLE 3. Crack Density Data of Westerly Granite at 50 MPa (Room Pressure)

Sample	$P_L^{\perp}$,* mm^{-1}	$P_L^{\parallel}$,* mm^{-1}	S_V,† mm^2/mm^3	M,# 10^4 J m^{-3}	W,§ 10^4 J m^{-3}	Comments
T0	4.82	4.91	9.68	0	0	virgin sample
T5	8.85	5.71	16.35	0.67–6.67	6 ± 3	sample retrieved just before failure

* Data of Tapponnier and Brace [1976].
† Calculated from equation (8).
# Calculated from equation (5).
§ Calculated from equation (1).

single preferred orientation (σ_1) and that P_L as a function of θ (angle between the crack and σ_1) is given by

$$P_L(\theta) = a + b \sin\theta \qquad (8a)$$

with

$$a = P_L^{||} \text{ and } b = P_L^{\perp} - P_L^{||}$$

The crack surface per unit volume for such a distribution is given by [Underwood, 1970]

$$S_V = \pi/2\ P_L^{\perp} + (2 - 2/\pi)P_L^{||} \qquad (8b)$$

The calculated values are shown in Table 3. Referring to (5), we therefore have S_V = 16.35 mm^2/mm^3 and S_V^0 = 9.68 mm^2/mm^3; 2Γ in quartz and feldspars ranges from 1 J m^{-2} to 10 J m^{-2} [Brace and Walsh, 1962; Atkinson, 1979]. A reasonable estimate of M is therefore 6.67 x 10^3 to 6.67 x 10^4 J m^{-3}.

Post-failure Data

Two series of post-failure experiments at 80 MPa and 250 MPa were performed; the details have been described by Wong [1981a]. In addition, a number of room temperature post-failure studies have been reported in the literature. G for Westerly granite [Wawersik and Brace, 1971; Wong, 1981a] and Oshima granite [Sano, 1978] were calculated by us; that for Fichtelgebirge granite [Rummel et al., 1978] was calculated by Rice [1980] (Table 2 and Figure 3). Values of Δu and ω_0 were also computed; all calculations are based on equations (2), (3), and (4).

The lower limit of integration in (2) depends on our picks of the residual stress level τ^f. As is evident from the post-failure data of Wong [1981a], the transition to stable sliding is rather gradual owing to the tendency of the jacket to hinder the sliding motion. This is the major source of experimental error. Taking into consideration the error due to numerical integration, we judge the estimation of G to be accurate probably within a factor of 2.

We also counted the cracks under the SEM for three post-failure samples from our previous study [Wong, 1981b]. The samples P4, P6, and P7 were all deformed at 150°C and 250 MPa. Referring to Figure 1 of Wong [1981b], P4 is a sample retrieved immediately after failure, whereas P6 and P7 experienced a differential stress drop of about 75 MPa and 120 MPa, respectively. The total stress drop to reach the residual stress level is about 350 MPa.

In P4, several areas with intergranular cracking extending over three or four grains can be located. We counted the cracks in a mosaic covering a localized zone of length of about 2.3 mm. A more detailed description of this area was given by Wong [1981b]; as was pointed out there, the zone was the most extensive one we located in the sample, and the crack counts should be higher than the average value in the sample. We chose for P6 a representative area along one of the two prominent localized zones, which is composed of a mixture of shear cracks and crack arrays and networks. It was obvious at high magnification (above 1000X) that

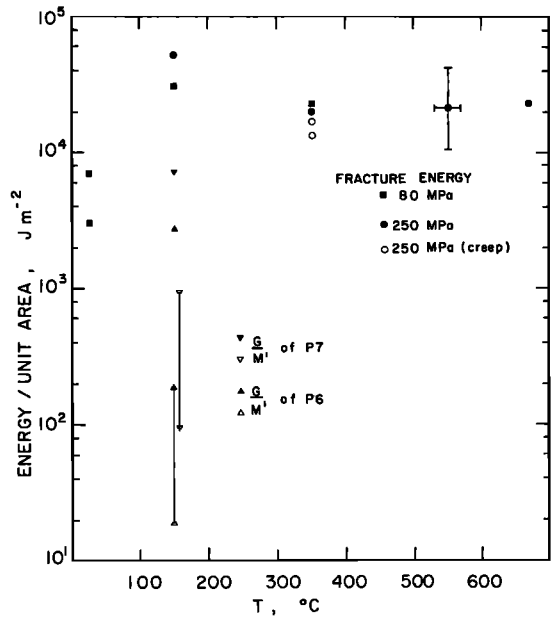

Fig. 3. Variation of shear fracture energy G with temperature at constant pressures of 80 MPa and 250 MPa. Bars are shown indicating estimated uncertainty in G and temperature measurements. Values of G and M^1 of the two post-failure samples P6 and P7 are also shown for comparison.

crushing into fine-grained particles started to occur along portions of the localized zone in P6, and extensive crushing in P7 was obvious even at 300X. For P7 we counted the cracks as seen on two more 'intact' areas along the incipient fault comprising all three major minerals. An unambiguous count of the cracks at a reasonable magnification along the 'crushed up' areas is impossible, and we expect our estimates for both P6 and P7 to be lower than the average value along the localized zone.

The crack intersections per unit length data in the post-failure samples P4 and P6 can be reasonably represented as

$$P_L(\theta) = a + b \sin\theta + c \sin|\theta-\omega| \qquad (9a)$$

where θ is the angle between the test array and σ_1, and ω that between the localized zone and σ_1 [Wong, 1981c]. Since the count in P7 was done on areas not quite representative of the localized zone (most of which tended to be more crushed), a detailed knowledge of $P_L(\theta)$ as seen on the mosaic would not be of much physical significance. We therefore only measured P_L in two orthogonal directions and used (8a) to estimate the crack length per unit area (L_A). For P4 and P6 we used the following relationship: $L_A = a/2 + b + c$; the crack surface per unit volume is then given by $S_V = L_A$ [Underwood, 1970; Wong, 1981c].

The calculated values are tabulated in Table 4, and referring to (6), we have S_V^f = 15.91 mm^2/mm^3, S_V^P = 24.13 and 58.30 mm^2/mm^3 for P6 and P7 respectively. Our SEM observation [Wong, 1981b] shows that a localized zone is seldom more than four grains wide, and since the areas covered by our mosaics were from two to three grains wide, we shall use a value of 3

TABLE 4. Crack Density Data of Westerly Granite at 250 MPa and 150°C

Sample	L,* mm	$P_L(\theta)$, mm^{-1}	S_V,† mm^2/mm^3	M^1,# 10^2 J m^{-2}	G,§ 10^3 J m^{-2}
P4	65	$7.95+2.30\sin\theta+1.12\sin\lvert\theta-30°\rvert$	15.91	0	0
P6	100	$9.22+4.89\sin\theta+4.76\sin\lvert\theta-20°\rvert$	24.13	0.19-1.85	2.7
P7	24	$19.29+28.00\sin\theta$	58.30	0.95-9.54	7.4

* Total length of test array. Magnification of the mosaics was 300X, and the spacing between adjacent traverses was 33 μm.
† Calculated from the equation: $S_V = L_A = a/2 + b + c$.
# Calculated from equation (6).
§ Calculated from equation (2) with fracture angle 30°. G estimated from the complete post-failure curve was 5.1×10^4 J m^{-2}.

times the grain size for the zone width. Since the average grain dimension of Westerly granite is 0.75 mm, we have $w \simeq 2.25$ mm. Substituting all these values into (6), we conclude that a reasonable estimate of a lower bound on M^1 is from 1.85×10^1 to 1.85×10^2 J m^{-2} for P6 and from 9.54×10^1 to 9.54×10^2 J m^{-2} for P7 (Table 4 and Figure 3).

In addition to the problem of resolving power of the SEM (which is limited to be above 0.02 μm) the major source of error in the determination of both M and M^1 is from the stereological procedures. When we counted the cracks, did we make the optimum choice of array spacing and angle increments to obtain a statistically meaningful sample of crack intersections? To what extent do the samples deviate from the type of symmetry in crack distribution we assumed? It is difficult at present to precisely determine the error in these procedures on the basis of our limited experience with the stereological methods. Techniques exist for exploring these questions [Underwood, 1970], and it would be useful to investigate the problem more thoroughly in the future.

Seismologically Inferred Values

In the past decade a number of studies have been made to determine G from seismological data; these results are compiled in Table 1a for comparison.

In addition, we determine G from McGarr et al.'s [1979] data on tremors in a deep gold mine (East Rand Proprietary Mines (E.R.P.M.) of the Witwatersrand in South Africa. Equation (7) is used with $\alpha = 1$. We can estimate R and $\Delta\tau$ in two ways. Following Husseini et al.'s [1975] approach and referring to Table 3 of McGarr et al. [1979], we get R = 215 m and $\Delta\tau = 0.75$ MPa solely on the basis of seismic data. On the other hand, if, as suggested by McGarr et al., we use the seismic moment and underground measurement of the average slip to infer R and $\Delta\tau$, we get R = 48 m and $\Delta\tau = 69.5$ MPa. Values of G so determined by us from these two sets of estimates are included in Table 1a.

Discussion

Role of Microcracking in Pre-failure and Post-failure Deformation

The data shown in the last two columns of Tables 3 and 4 show that the energy associated with microcracking (M and M^1) should, as expected, be smaller than the total energy input for pre-failure (W) and post-failure (G) deformation, respectively. Our data also show that the ratio M/W is significantly higher than M^1/G. Several factors may contribute to this difference. First, the location of the mosaics for the post-failure samples was deliberately chosen such that our estimates of S_V^P and S_V^f (equation (6)) would be lower and upper bounds, respectively; therefore our estimates are lower bounds on M^1, whereas for the pre-failure sample the estimate is a representative value for M as seen in the SEM. Second, the pressure and temperature were higher in P4-P7, possibly resulting in significant difference in values of Γ. Third, the variation can be due to an intrinsic difference between the energy budget for pre-failure deformation and that for post-failure deformation. Probably other energy sinks, such as frictional heating and acoustic emission, are more appreciable for the latter process.

The closeness in values for the two energy terms in the pre-failure sample T5 indicates that most of the stress-induced cracks are resolvable under the SEM. It was concluded by Hadley [1976] that pre-existing voids in Westerly granite may be seriously underestimated with SEM observation. However, if the tip of a given crack has taken up an appreciable amount of the energy input, it results in both widening and extension of the crack. Such cracks are more readily observed under the SEM.

Although we conclude from our SEM observations [Wong, 1981b] that extensive microcracking is involved in the faulting process and that a large portion of the cracks are axial ones formed in tension, the tensile fracture energy measurements are not the appropriate values for characterizing the shear fault formation. The data in Table 4 show that for a sample that is only about one-

third of the way into the post-failure region, the use of the tensile values would have underestimated the energy for microcracking alone by 1-2 orders of magnitude, depending on whether the single-crystal or pre-cracked rock value is used. The pre-cracked rock tensile measurements are, of course, very useful for engineering applications such as hydraulic fracturing; our calculation here also shows that the use of single-crystal tensile measurements to characterize cracks at a microscopic scale gives results consistent with the constraints on energy dissipation placed by the macroscopic stress and strain.

Comparison of Laboratory Measurements and Seismologically Inferred Values of the Shear Fracture Energy G

As is evident from Table 1a, the values from seismology can vary widely. For the 1966 Parkfield earthquake, which is unquestionably one of the best documented earthquakes, Husseini et al.'s [1976] estimate of G is 2.3×10^3 J m^{-2}, whereas Aki's [1979] estimate is 1.6×10^6 J m^{-2}. (We correct here a typographical error in the former paper which gives a low G value of 1 order of magnitude.) Husseini et al. estimated the rupture area by corner frequency analysis, which involves considerable uncertainty. The limitation of this approach was discussed in some detail by Rice [1980]; Aki [1979] also argued that this approach is biased toward an underestimate. On the other hand, Aki's estimate of rupture area hinges on the assumption of the barrier model, and the high value may be a consequence of this assumption [Rudnicki, 1980].

Considerable discrepancy also exists between two estimates of G for the 1857 Fort Tejon earthquake. Aki [1979] determined G for this large earthquake to be 2×10^8 J m^{-2}, whereas Rudnicki's [1980] estimate is 3.8×10^6 J m^{-2}. As discussed above, we calculated G for seismic events in E.R.P.M., South Africa. The two estimates are 1.0×10^3 J m^{-2} and 1.8×10^6 J m^{-2} (Table 1a). This set of values is particularly interesting because the seismicity is not associated with pre-existing faults and should, in this sense, be very similar to brittle fracture of intact samples in the laboratory [McGarr et al., 1979]. The country rock at E.R.P.M. is Witwatersrand quartzite. We determined G from laboratory measurements of post-failure behavior presented by Spottiswoode [1980]. Using (2), values of G for the quartzite from the post-failure curves are 0.8×10^4 J m^{-2} and 1.3×10^4 J m^{-2}. The laboratory values fall between the two seismologically inferred values.

The experimental values determined from post-failure curves (Table 2) for both initially intact and pre-fractured samples are all of the order of 10^4 J m^{-2}. The shear G value determined experimentally is therefore roughly 2 orders of magnitude higher than the tensile measurements. The former compares more favorably with the seismologically inferred values, but the discrepancy can still amount to 3 orders of magnitude.

Estimates of ω_0 compiled in Table 2 suggest that our calculation of G based on laboratory data should only be considered as an approximation. Over the pressure and temperature range we considered, ω_0 is of the order of tens of centimeters. This indicates that in centimeter-size rock sample, slip occurs almost simultaneously along the localized zone, rather than in a crack-like mode as assumed in the model (Figure 2). Nevertheless, the integral in (2) should be valuable for order-of-magnitude estimates.

The room temperature laboratory G measurements can be separated into two groups: Westerly and Oshima granite and Witwatersrand quartzite have lower G, whereas the 'softer' Fichtelgebirge granite tends to have significantly higher values. At comparative pressures the latter can be higher by 1 order of magnitude; this may be indicative of the extent of variation with rock type to be expected of G.

For the same rock type (Westerly granite) the effect of pressure and temperature can increase G by an order of magnitude. We plot all the data on Westerly granite at 80 MPa and 250 MPa in Figure 3 to illustrate the variation of G with temperature. At 80 MPa, G first increases with temperature and then decreases. At 250 MPa and temperatures above 350°C the relative increase in slip and reduction in stress drop accompanying a temperature increase compensate for each other, so that G as determined from the integral in (2) remains roughly constant.

We have data at only two pressures. Furthermore, the normal stress on the localized zone is not constant but decreases during slip in an experiment. It would therefore be difficult to generalize on pressure effects. For the room temperature data, no systematic trend can be detected from Wawersik and Brace's [1971] data, although Rummel et al.'s [1978] results show a twofold increase of G from 55 MPa to 157 MPa, similar to the increase with pressure in our 150°C data.

If we try to determine G from the post-creep failure curves with the assumption that localization occurs at the onset of tertiary creep and that (2) applies, then the G values for the two creep specimens (PFW 17 and PFW 27) with different loading history [Wong, 1981a] agree quite well. The creep values are lower than the value for PEW 16 deformed at the same temperature and pressure but at constant displacement rate. This comparison may not be appropriate because two different assumptions have been made concerning the point of localization for the two different types of loading.

An implicit assumption of strain rate independence has been made in deriving (2). Stesky [1978] reported that in faulted samples deformed under 250 MPa pressure a sharp increase in dislocation density and strain rate sensitivity was observed at about 500°C. This limitation ought to be noted for our estimates for G at temperatures higher than about 500°C. Furthermore, fracture mechanics tests on rocks and minerals in a tensile mode have concluded that water can influence the critical parameters significantly through the stress-corrosion mechanism [Atkinson, 1979]. We did not investigate systematically the effect of pore fluid on post-failure behavior and shear fracture energy. It would be

speculative to infer the extent of this effect by extrapolating the mode I results to Mode II.

Conclusion

In recent years, extensive work has been done on these four separate areas: the estimation of shear fracture energy from seismological data, the laboratory study of post-failure behavior in triaxial compression, the measurement of tensile specific surface energy of single crystals, and the observation of stress-induced microstructures under the SEM. We have attempted to gain a better understanding of the relationship among the four different types of measurements from energetic considerations.

Previous work has shown that quantitative information on the effects of cracks on physical quantities such as velocity [Hadley, 1976] and permeability [Brace, 1977] can be extracted from careful SEM observation. The present study shows that SEM observation is useful for the estimation of energy associated with the microcracking process. We also demonstrate the feasibility of a systematic application of stereological techniques for acquisition of reasonably accurate crack area data.

The fracture energy concept has long been proved to be a powerful tool in engineering fracture mechanics, and the potential for application of similar concepts to fault mechanics is evident in the numerous recent attempts to use fracture mechanics in theoretical models. We conclude on the basis of our study of post-failure behavior [Wong, 1981] that the variability of the load-displacement curve due to both loading history and statistical differences among specimens suggests the use of a global physical quantity such as G for the characterization of post-failure behavior.

However, even in the laboratory context there still exist several difficulties in applying the concept. For initially intact samples a better understanding of the 'slip-weakening' process on a microscopic level is necessary before we can locate the onset of shear localization and model the complex process better. Rice's calculation shows that G of a pre-fractured sample is of the same order as that of an initially intact sample. However, it is only fair to say that unlike the case of post-failure behavior of initially unfractured rock, the dependence of details of frictional behavior on testing machine characteristics and the relationship of stick-slip with respect to machine stiffness are questions not fully understood [Byerlee and Brace, 1968; Ohnaka, 1975; Ida, 1975; Goodman and Sundaram, 1978]. The principal problem for application of Rice's theory to pre-fractured samples may therefore not lie with the location of the first integration limit in (2) (the point of localization) but with the second limit, namely, the question of whether the sample has 'overshot' and what the residual stress level should be.

Nevertheless, an estimate of the fracture energy under shear in a triaxial configuration is clearly more realistic for fault mechanics application than values measured in a tensile mode. That the laboratory G measurements in shear agree more favorably with seismologically inferred values than the tensile measurements is encouraging. The data compiled by us show that the effects of temperature and pressure and different rock types can change G by an order of magnitude. It will be useful to investigate this in greater detail and see to what extent we can generalize the effect of pressure and temperature to pre-fractured samples and over a broad range of rock types. To what extent these data can be applied to field situations, of course, still hinges on a better understanding of the important problem of scaling.

Acknowledgments. I am grateful to W. F. Brace for his patient guidance and encouragement throughout the course of this work. I would like to thank K. Aki, J. R. Rice, and J. B. Walsh for valuable suggestions and comments. This research was supported by the National Science Foundation under grants EAR77-23158, EAR79-10854, and EAR80-25369.

References

Aki, K., Characterization of barriers on an earthquake fault, J. Geophys. Res., 84, 6140-6148, 1979.

Aki, K., and P. G. Richards, Quantitative Seismology, W. H. Freeman, San Francisco, Calif., 1980.

Atkinson, B. K., Compilation of experimentally determined fracture mechanics parameters for geological materials, final technical report, U.S. Natl. Earthquake Hazards Reduction Program, Imperial College, London, U.K., 141 pp., 1979.

Barenblatt, G. I., The mathematical theory of equilibrium cracks in brittle fracture, Adv. Appl. Mech., 7, 55-129, 1962.

Brace, W. F., Permeability from resistivity and pore shape, J. Geophys. Res., 82, 3343-3349, 1977.

Brace, W. F., and J. B. Walsh, Some direct measurements of the surface energy of quartz and orthoclase, Am. Mineral., 47, 1111-1122, 1962.

Brace, W. F., B. Paulding, and C. H. Scholz, Dilatancy in the fracture of crystalline rocks, J. Geophys. Res., 71, 3939-3954, 1966.

Brune, J. N., Tectonic stress and the spectra of seismic shear waves from earthquakes, J. Geophys. Res., 75, 4997-5009, 1970. (Correction, J. Geophys. Res., 76, 5002, 1971.)

Byerlee, J. D., and W. F. Brace, Stick-slip, stable sliding and earthquakes: Effect of rock type, pressure, strain rate, and stiffness, J. Geophys. Res., 73, 6031-6037, 1968.

Das, S., A numerical study of rupture propagation and earthquake source mechanism, Ph.D. thesis, Mass. Inst. of Technol., Cambridge, 1976.

Freiman, S. W., Fracture Mechanics Applied to Brittle Materials, STP678, Am. Soc. for Testing & Matls., Philadelphia, Pa., 1979.

Freund, L.B., The mechanics of dynamic shear crack propagation, J. Geophys. Res., 84, 2199-2209, 1979.

Friedman, M., J. Handin, and G. Alani, Fracture surface energy of rocks, Int. J. Rock Mech. Min. Sci., 9, 757-766, 1972.

Goodman, R. E., and P. N. Sundaram, Fault and system stiffness and stick slip phenomena, Pure Appl. Geophys., 116, 873-887, 1978.

Hadley, K., Comparison of calculated and observed crack densities and seismic velocities in

Westerly granite, J. Geophys. Res., 81, 3484-3493, 1976.
Hallbauer, D. K., H. Wagner, and N. G. W. Cook, Some observations concerning the microscopic and mechanical behavior of quartzite specimens in stiff, triaxial compression tests, Int. J. Rock Mech. Min. Sci., 10, 713-726, 1973.
Hudson, J. A., E. T. Brown, and C. Fairhurst, Optimizing the control of rock failure in servo-controlled laboratory tests, Rock Mech., 3, 217-224, 1971.
Husseini, M. I., D. B. Jovanovich, M. J. Randall, and L. B. Freund, The fracture energy of earthquakes, Geophys. J. R. Astron. Soc., 43, 367-385, 1975.
Ida, Y., Cohesive force across the tip of a longitudinal shear crack and Griffith's specific surface energy, J. Geophys. Res., 77, 3796-3805, 1972.
Ida, Y., The maximum acceleration of seismic ground motion, Bull. Seismol. Soc. Am., 63, 959-968, 1973.
Ida, Y., Analysis of stick slip and earthquake mechanism, Phys. Earth Planet. Inter., 11, 147-156, 1975.
Kendall, M. G., and P. A. P. Moran, Geometric Probability, Charles Griffin, London, 1963.
Kranz, R. L., Crack growth and development during creep in Barre granite, Int. J. Rock Mech. Min. Sci., 16, 23-36, 1979.
Kranz, R. L., The effects of confining pressure and stress difference on static fatigue of granite, J. Geophys. Res., 85, 1854-1866, 1980.
Lockner, D. A., and J. D. Byerlee, Microfracturing and velocity changes during creep in granite (abstract), EOS, Trans. AGU., 59, 1207, 1978.
McGarr, A., S. M. Spottiswoode, N. C. Gay, and W. D. Ortlepp, Observations relevant to seismic driving stress, stress drop, and efficiency, J. Geophys. Res., 84, 2251-2261, 1979.
Ohnaka, M., Frictional characteristics of typical rocks, J. Phys. Earth, 23, 87-112, 1975.
Palmer, A. C., and J. R. Rice, The growth of slip surfaces in the progressive failure of over-consolidated clay, Proc. R. Soc. London, Ser. A, 332, 527-548. 1973.
Rice, J. R., A path independent integral and the approximate analysis of strain concentration by notches and cracks, J. Appl. Mech., 35, 379-386, 1968.
Rice, J. R., The mechanics of earthquake rupture, in Physics of the Earth's Interior, edited by A. M. Dziewonski and E. Boschi, p. 555-649, Italian Physical Soc., Bologna, Italy, 1980.
Rice, J. R., and D. A. Simons, The stabilization of spreading shear faults by coupled deformation-diffusion effects in fluid-infiltrated porous materials, J. Geophys. Res., 81, 5322-5334, 1976.
Rudnicki, J. W., Fracture mechanics applied to the earth's crust, Annu. Rev. Earth Planet., 8, 489-525, 1980.
Rummel, F., H. J. Alheid, and C. Frohn, Dilatancy and fracture-induced velocity changes in rock and their relation to frictional sliding, Pure Appl. Geophys., 116, 743-764, 1978.
Sano, O., Fundamental study on the mechanisms of brittle fracture of rocks, D. Eng. thesis, Kyoto Univ., Kyoto, Japan, 1978.
Soga, N., H. Mizutani, H. Spetzler, and R. J. Martin III, The effect of dilatancy on velocity anisotropy in Westerly granite, J. Geophys. Res., 83, 4451-4458, 1978.
Spottiswoode, S. M., Fault gouge, driving stress, and seismic efficiency, submitted to J. Geophys. Res., 1980.
Stesky, R. M., Mechanism of high temperature frictional sliding in Westerly granite, Can. J. Earth Sci., 15, 361-375, 1978.
Takeuchi, H., and M. Kikuchi, A dynamical model of crack propagation, J. Phys. Earth, 21, 27-37, 1973.
Tapponnier, P., and W. F. Brace, Development of stress-induced microcracks in Westerly granite, Int. J. Rock Mech. Min. Sci., 13, 103-112, 1976.
Underwood, E. E., Quantitative Stereology, Addison-Wesley, Reading, Pa., 1970.
Wawersik, W. R., and C. Fairhurst, A study of brittle rock fracture in laboratory compression experiments, Int. J. Rock Mech. Min. Sci., 7, 561-575, 1970.
Wawersik, W. R., and W. F. Brace, Post-failure behavior of a granite and a diabase, Rock Mech., 3, 61-85, 1971.
Wong, T.-F., Effect of temperature and pressure on failure and post-failure behavior of Westerly granite, Mech. Mater., in press, 1981a.
Wong, T.-F., Micromechanics of faulting in Westerly granite, Int. J. Rock Mech. Min. Sci., in press, 1981b.
Wong, T.-F., Development of stress-induced anisotropy and localized deformation in brittle rock, in Plastic Behavior of Anisotropic Solids, Centre National de la Recherche Scientifique, Villard-de-Lans, in press, 1981c.

(Received February 10, 1981;
revised August 6, 1981,
accepted September 25, 1981.)